

Newton-Euler Based Dynamic Modeling and Control Simulation for Dual-Axis Parallel Mechanism Solar Tracker

Sarot Srang^{*,1}, Sopagna Ath², Masaki Yamakita²

¹*Institute of Technology of Cambodia, Industrial and Mechanical Engineering Department, 12150, Cambodia*

²*Tokyo Institute of Technology, Systems and Control Engineering Department, 152-8552, Japan*

ARTICLE INFO

Article history:

Received: 24 July, 2020

Accepted: 25 September, 2020

Online: 05 October, 2020

Keywords:

Parallel Mechanism

Kinematic Constrained

Euler Parameters

Cartesian Coordinate System

Algebraic Differential Equations

ABSTRACT

Dynamic modeling has been a crucial study in many areas of the engineering field. In this paper, we apply the Newton-Euler equation of motion to a two-DOF parallel mechanism solar tracker which is a close loop mechanism. The aim of this study is to show a simulation of the dynamical model with feedback control using a PD controller to orientate the solar panel perpendicular to the sun rays. The mechanism is modeled in the form of a system of algebraic differential equations. First, kinematic constraint equations were constructed in the form of algebraic equations to specify the dynamic interactions at joints. We use the Baumgarte stabilization method, a constraint violation method to eliminate computational error incurred by numerical approximation. Then, the dynamic equations of the system were formulated using the Newton-Euler equation of motion. To describe the translation and rotation motions, we apply Cartesian coordinates and Euler parameters. Simulation of driving the solar panel to reach the desired configuration is made, and the result shows that the PD controller provides good performance of the mechanism regardless of the complexity of the dynamic behavior of the mechanism.

1 Introduction

This paper is an extension of work originally presented in 2019 *IEEE/ASME International Conference on Advanced Intelligent Mechatronics (AIM). IEEE, 2019* [1]. Solar energy has been a major current research in the electricity generation field because of its unlimited resource and environmental friendly behavior. The efficiency of solar energy can be improved by implementing a tracking mechanism which keeps the solar panel perpendicular to the sun rays. There exists two main types of tracking mechanism, a single and dual axis solar tracker [2]. Energy gain from a single axis solar tracker was reported to be 20% [3] while energy gain from a dual axis solar tracker was 30-40% [4].

Dual axis solar tracker has been of an interest research topic for many researchers, [3], [5]–[7], because of its outperformance over single axis solar tracker. Many researches on energy gain from solar tracking systems compared to the tilted fixed panel had been done both theoretically and experimentally [5]. In [7], the author proposed a two-axis decoupled solar tracking system based on parallel mechanism and showed that the tracker requires less driving torque,

thus less power dissipation than the conventional serial tracker does. Furthermore, the tracking system does not need reducer with large reduction ratio. Therefore, complexity and weight of the system are also reduced. The parallel mechanism solar tracker can be implemented by mounting on either a fixed or moving platform to produce electrical energy. For instance, aerial vehicles, boats, land vehicles are considered as moving platform. Assuming that the parallel mechanism solar tracker is attached to an aerial vehicle, the dynamic effect must be taken into account. The scope of this study is limited to a fixed platform.

Various methods for dynamic modeling for mechanical systems have been widely developed, and each one has its own advantages and disadvantages. In general, dynamic modeling using generalized coordinate (e.g. Lagrange's dynamic equation) yields the smallest number of differential equations and, therefore, computational efficient. However, the order of nonlinearity is high, and derivation of equation in expanded form of multibody system with loops of connected links is very tedious. For parallel mechanism, derivation can be done by virtually decomposing the system as open loop mechanism with some kinematic constraint forces by the other

*Corresponding Author: Sarot Srang, Department of Industrial and Mechanical Engineering, Institute of Technology of Cambodia, Russian Federation Blvd., P.O.Box 86, Sangkat Tuek L'ak 1, Khan Tuol Kouk, Phnom Penh, Cambodia. srangsarot@itc.edu.kh

parts of the system. For a system with more than one loop like the tracker we are considering, the derivation is even more difficult, and only partial reaction (or constraint) forces can be determined. With cartesian coordinates in global and body-fixed frames and Euler parameters for describing rotation, dynamic modeling using Newton's method is much simpler, and systematic generation of kinematic constraints at all joints and dynamic equations can be derived easily [8]. The method yields system equations of algebraic-differential equations. Reaction forces and the coordinates describing motion of a system are obtained from solving the equations. The reaction force has an advantage for mechanical structure design. A high-performance computer can realize the simulation modeled in detail including the reaction force effect in this case. However, the analysis of reaction forces is not reported in this work.

The remaining contents of this paper are organized as follows. In section 2, the parallel mechanism is explained on configuration, and its kinematic is described by using Cartesian coordinate. Dynamic equations for unconstrained and constrained body which are described in Cartesian coordinate and using Euler parameters are given in section 3. For constrained body, the resulted equation is in the form of system algebraic-differential equations. In section 4, the controller design is covered by using PD controller. Section 5 presents the results and discussion. We conclude our paper in section 6.

2 Kinematic Constraint

Cartesian coordinate is used to describe the system configuration, and constraint equations are obtained from individual joints. Figure 1 shows the coordinate system, where $(Oxyz)$ is global frame and $(O_i\xi_i\eta_i\zeta_i)$ is body-fixed frame attached on body i with the center of mass O_i . A point P on the body has coordinate as a vector in body-fixed frame and global frame defined by s_i^P and r_i^P respectively. Figure 2 shows a parallel mechanism which is used as dual axis solar tracker. The body numbers are labeled as seen in the figure. The mechanism consists of 7 connected rigid bodies. It has a global coordinate $(Oxyz)$, and each body has its own body-fixed frame as explained in Figure 2. Body 7 is connected with body 5 and 6 via 2 spherical joints and with body 4 via a universal joint. Body 6 is connected with body 2 via a revolute joint. Body 5 is connected to body 3 via a universal joint. Body 4 is connected to body 1 (ground) via another revolute joint. Body 3 is connected with body 1 via a translational joint. Body 2 is connected with body 1 via another translational joint. Two linear actuators are attached at the translational joints. The actuators exert forces on body 2 and 3 along vertical axes.

Denote $q_i = [r_i^T, p_i^T]^T = [x, y, z, e_0, e_1, e_2, e_3]^T$ as a coordinate vector of the body i , where r_i is position vector of the center of mass of the body as illustrated in Figure 1, and $p_i = [e_0, e^T]^T = [e_0, e_1, e_2, e_3]^T$ is Euler parameters.

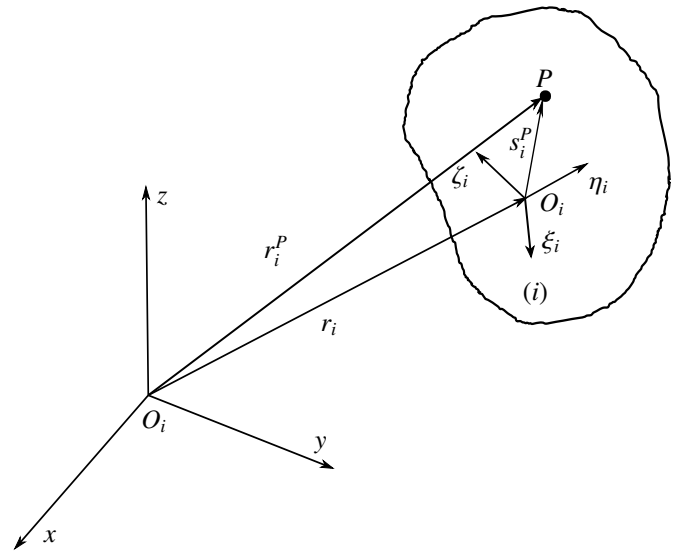


Figure 1: Cartesian Coordinate System

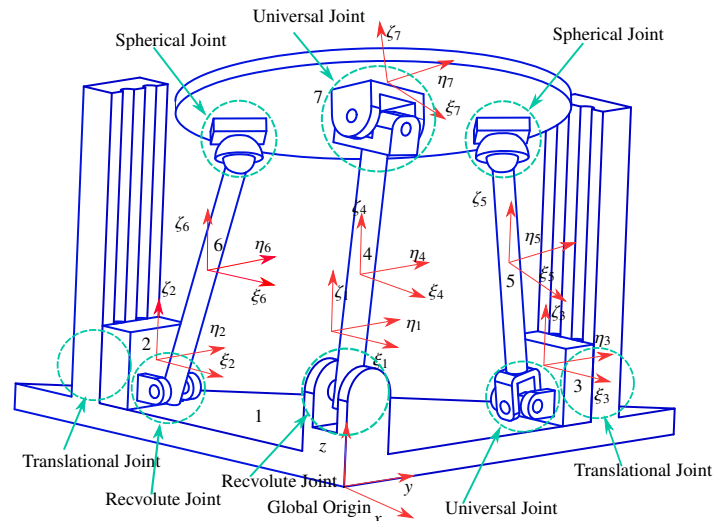


Figure 2: Global and Local coordinates of the parallel mechanism at the initial configuration

The parameter satisfies a mathematical relationship,

$$p_i^T p_i - 1 = 0. \quad (1)$$

The second time derivative of (1) is

$$p_i^T \ddot{p}_i + \dot{p}_i^T \dot{p}_i = 0. \quad (2)$$

Denote R_i as a rotational matrix of body i , and a pair of 3×4 matrices G_i and L_i defined as $G_i = [-e, \tilde{e} + e_0 I]_i$ and $L_i = [-e, -\tilde{e} + e_0 I]_i$. Then $R_i = G_i L_i^T$, [8]. The global coordinate of the point P illustrated in Figure 1 can be defined by

$$r_i^P = r_i + R_i s_i^P = r_i + G_i L_i^T s_i^P, \quad (3)$$

where $s_i^P = [\xi^P, \eta^P, \zeta^P]^T$ is body-fixed coordinate of the point P .

Denote $q = [q_1^T, q_2^T, q_3^T, q_4^T, q_5^T, q_6^T, q_7^T]^T$ as coordinate vector for describing the configuration of the mechanism, and its respective first and second time derivative, \dot{q} and \ddot{q} , for describing the motion of the mechanism. The number of coordinates of the system is $n = 7 \times 7 = 49$, and the number of Euler parameters relationship (or mathematical constraint) is 7.

Denote

$$\Phi \equiv \Phi(q) = 0 \quad (4)$$

as kinematic equation derived from kinematic constraints which have 34 equations. The compact form of the kinematic equation for each joint is given in Appendix A. The first and second time derivative of (4) are written as

$$\begin{aligned} \Phi_q \dot{q} &= 0, \\ \Phi_q \ddot{q} + (\Phi_{qq} \dot{q}) \dot{q} &= 0 \\ \text{or } \Phi_q \ddot{q} &= \gamma, \end{aligned} \quad (5)$$

where $\gamma = -(\Phi_{qq} \dot{q}) \dot{q}$ is called the right side of the kinematic acceleration equation and can be found in [8]. We adopt the constraint violation stabilization methods from [9], another similar technique can also be found in [10, 11].

Consider the following closed loop system,

$$\ddot{D} + K_P \dot{D} + K_D D = 0, \quad (6)$$

where K_P and K_D are constant and defined in Appendix B. Due to the fact that there exists numerical errors in using numerical method to solve the differential equations (5), we use the positive constraint violation stabilization method to obtain a stable response. So (5) is modified such that the kinematic constraint equations are satisfied by ensuring the shrinking of the computation error.

First time derivative of constraint equation is obtained as

$$\Phi_q \dot{q} = \dot{D} \quad (7)$$

Second time derivative of the constraint equation is given as

$$\begin{aligned} \Phi_q \ddot{q} + (\Phi_{qq} \dot{q}) \dot{q} &= \ddot{D} \\ &= -K_D \dot{D} - K_P D \\ &= -K_D (\Phi_q \dot{q}) - K_P \Phi(q) \end{aligned} \quad (8)$$

Thus,

$$\Phi_q \ddot{q} = \gamma - K_D (\Phi_q \dot{q}) - K_P \Phi(q). \quad (9)$$

The equation (9) is used for simulation and the performance is discussed in section 5.

3 Dynamic Modeling for Unconstrained and Constrained Bodies

Newton-Euler equations of motion is used to derive the equations of motion for multi-rigid bodies of the parallel mechanism. Prior to having the equations of motion for a set of interconnected bodies by kinematic joints which is known as constrained body, the equations of motion for body with no contact to other bodies which refers as an unconstrained body are written.

3.1 Dynamic Equations for Unconstrained Bodies

From Newton's method, an unconstrained body i with mass m_i and moment of inertia J'_i with respect to its center of mass exerted by external force f_i and moment τ'_i has dynamic equation of motion as

$$\begin{aligned} N_i \ddot{r}_i &= f_i \\ J'_i \dot{\omega}'_i + \tilde{\omega}'_i J'_i \omega'_i &= n'_i, \end{aligned} \quad (10)$$

where $N_i = \text{diag}([m \quad m \quad m])_i$ and ω'_i is the angular velocity defined in body-fixed frame. The equation of rotational motion in (10) is transformed by using the following relationships [8].

$$\begin{aligned} \omega' &= 2L\dot{p} \\ \dot{\omega}' &= 2L\ddot{p}. \end{aligned} \quad (11)$$

$$\widetilde{L_i \dot{p}_i} = L_i \dot{L}_i^T \quad (12)$$

Equation (10) becomes

$$\begin{aligned} 2J'_i L_i \ddot{p}_i + 4\widetilde{L_i \dot{p}_i} J'_i L_i \dot{p}_i &= n'_i \\ 2J'_i L_i \ddot{p}_i + 4L_i \dot{L}_i^T J'_i L_i \dot{p}_i &= n'_i \\ 2J'_i L_i \ddot{p}_i + L_i H_i \dot{p}_i &= n'_i, \end{aligned} \quad (13)$$

where $H_i = 4L_i^T J'_i L_i$. The dynamic equations of motion for an unconstrained bodies are written as

$$\begin{aligned} N_i \ddot{r}_i &= f_i \\ 2J'_i L_i \ddot{p}_i + L_i H_i \dot{p}_i &= n'_i \\ p_i^T \ddot{p}_i + \dot{p}_i^T \dot{p}_i &= 0. \end{aligned} \quad (14)$$

In matrix form, (14) is rewritten as

$$\begin{bmatrix} N_i & 0 & 0 \\ 0 & 2J'_i L_i & 0 \\ 0 & p_i^T & 0 \end{bmatrix} \begin{bmatrix} \ddot{r}_i \\ \ddot{p}_i \\ 0 \end{bmatrix} + \begin{bmatrix} 0 \\ L_i H_i \dot{p}_i \\ \dot{p}_i^T \dot{p}_i \end{bmatrix} = \begin{bmatrix} f_i \\ n'_i \\ 0 \end{bmatrix}. \quad (15)$$

3.2 Dynamic Equations for Constrained Bodies

Bodies are interconnected to form a system of constrained bodies via kinematic joints which create constraint reaction forces and moments. When applying the constraint reaction forces and moments to (14), the dynamic equations of motion for a constrained bodies are written as

$$\begin{aligned} N_i \ddot{r}_i &= f_i + f_i^{(c)} \\ 2J'_i L_i \ddot{p}_i + L_i H_i \dot{p}_i &= n'_i + n'^{(c)}_i \\ p_i^T \ddot{p}_i + \dot{p}_i^T \dot{p}_i &= 0. \end{aligned} \quad (16)$$

A constrained body i is additionally exerted by reaction forces and moments $[f^{(c)}, n'^{(c)}]_i^T$ from joints. These forces and moments can be transformed to coordinate system consistent with q denoted by $[f^{*(c)}, n^{*(c)}]_i^T$ and defined by

$$\begin{bmatrix} f^{*(c)} \\ n^{*(c)} \end{bmatrix}_i = \begin{bmatrix} \Phi_r^T \\ \Phi_p^T \end{bmatrix}_i \lambda \quad (17)$$

To be used with the formulation (16), the moment in (17) is transformed to be

$$\begin{aligned} n^{(c)} &= \frac{1}{2} L_i n'^{(c)} \\ &= \frac{1}{2} L_i \Phi_{p_i}^T \lambda \end{aligned} \quad (18)$$

where $\lambda = [\lambda_1, \dots, \lambda_{34}]$ is known as Lagrange Multipliers, and $[\Phi_{r_i}, \Phi_{p_i}] = \Phi_{q_i}$ is Jacobian Matrix of the kinematic constraint $\Phi \equiv \Phi(q)$ with respect to q_i . Therefore, the dynamic equations of motion for the mechanism are given in compact form as

$$\begin{bmatrix} N_i & 0 & \Phi_{r_i}^T \\ 0 & 2J'_i L_i & \frac{1}{2} L_i \Phi_{p_i}^T \\ 0 & p_i^T & 0 \end{bmatrix} \begin{bmatrix} \ddot{r}_i \\ \ddot{p}_i \\ -\lambda \end{bmatrix} + \begin{bmatrix} 0 \\ L_i H_i \dot{p}_i \\ \dot{p}_i^T \dot{p}_i \end{bmatrix} = \begin{bmatrix} f_i \\ n'_i \\ 0 \end{bmatrix}. \quad (19)$$

$$\begin{bmatrix} M & B^T \\ P & 0 \end{bmatrix} \begin{bmatrix} \ddot{q} \\ -\lambda \end{bmatrix} + \begin{bmatrix} b \\ c \end{bmatrix} = \begin{bmatrix} g \\ 0 \end{bmatrix}, \quad (20)$$

where

$$M = \begin{bmatrix} N_1 & 0 & \dots & 0 & 0 \\ 0 & 2J'_1 L_1 & \dots & 0 & 0 \\ \vdots & \vdots & \ddots & \vdots & \vdots \\ 0 & 0 & \dots & N_7 & 0 \\ 0 & 0 & \dots & 0 & 2J'_7 L_7 \end{bmatrix},$$

$$B = [\Phi_{r_1}, \frac{1}{2} \Phi_{p_1} L_1^T, \dots, \Phi_{r_7}, \frac{1}{2} \Phi_{p_7} L_7^T]$$

$$P = \begin{bmatrix} 0^T & p_1^T & \dots & 0^T & 0^T \\ \vdots & \vdots & \ddots & \vdots & \vdots \\ 0^T & 0^T & \dots & 0^T & p_7^T \end{bmatrix}, b = \begin{bmatrix} 0 \\ L_1 H_1 \dot{p}_1 \\ \vdots \\ 0 \\ L_7 H_7 \dot{p}_7 \end{bmatrix}, c = \begin{bmatrix} \dot{p}_1^T \dot{p}_1 \\ \vdots \\ \dot{p}_7^T \dot{p}_7 \end{bmatrix},$$

$$g = \begin{bmatrix} f_1 \\ n'_1 \\ \vdots \\ f_7 \\ n'_7 \end{bmatrix}, \text{ and } \ddot{q} = [\ddot{r}_1^T \quad \ddot{p}_1^T \quad \dots \quad \ddot{r}_7^T \quad \ddot{p}_7^T]^T =$$

$$[\ddot{x}, \ddot{y}, \ddot{z}, \ddot{e}_0, \ddot{e}_1, \ddot{e}_2, \ddot{e}_3]^T, \quad (i = 1, 2, \dots, 7).$$

Equation (19) consists of 49 equations with 83 variables, therefore 34 constraint equations are appended with (19) to solve for coordinate vectors q and Lagrange multiplier λ . A system of algebraic differential equation is obtained as follow

$$\begin{bmatrix} M & B^T \\ P & 0 \\ \Phi_q & 0 \end{bmatrix} \begin{bmatrix} \ddot{q} \\ -\lambda \end{bmatrix} + \begin{bmatrix} b \\ c \\ 0 \end{bmatrix} = \begin{bmatrix} g \\ 0 \\ \gamma - K_D(\Phi_q \dot{q}) - K_P \Phi(q) \end{bmatrix}. \quad (21)$$

Equation (21) were solved for the coordinate vectors q by using state equations as follow:

$$x_1 = q = [x_1, y_1, z_1, [e_0, e_1, e_2, e_3]_1, \dots, x_7, y_7, z_7, [e_0, e_7, e_7, e_7]_7]$$

$$x_2 = \dot{q} = [\dot{x}_1, \dot{y}_1, \dot{z}_1, [\dot{e}_0, \dot{e}_1, \dot{e}_2, \dot{e}_3]_1, \dots, \dot{x}_7, \dot{y}_7, \dot{z}_7, [\dot{e}_0, \dot{e}_1, \dot{e}_2, \dot{e}_3]_7]$$

$$\dot{x}_1 = x_2 = \dot{q}$$

$$\dot{x}_2 = \ddot{q} = \begin{bmatrix} [I] & [0] \end{bmatrix} \begin{bmatrix} M & B^T \\ P & 0 \\ \Phi_q & 0 \end{bmatrix}^{-1} \begin{bmatrix} g - b \\ -c \\ \gamma - K_D(\Phi_q \dot{q}) - K_P \Phi(q) \end{bmatrix} \quad (22)$$

4 PD Controller

The desired value of actuator's displacement is obtained from the 3D model such that the solar panel reach the position as shown in Figure 4 where the desired value of the two actuators are $z_{2d} = 0.046m$, $z_{3d} = 0.046m$. The actual displacement of the two actuators labeled as body number 2 and body number 3 are denoted as z_2 and z_3 respectively. Figure 3 illustrates a common feedback controller known as proportional derivative (PD) controller that is used to obtain the desired response, and has a form as follow:

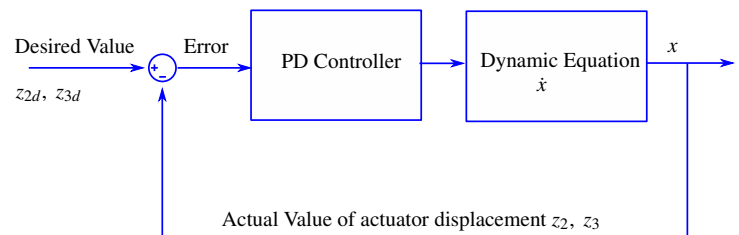


Figure 3: Block Diagram for PD Controller

$$u = K_p e_z + K_d \dot{e}_z, \quad (23)$$

where $u = \begin{bmatrix} f_{2z} \\ f_{3z} \end{bmatrix}$, $e_z = \begin{bmatrix} z_2 - z_{2d} \\ z_3 - z_{3d} \end{bmatrix}$ and $\dot{e}_z = \begin{bmatrix} \dot{z}_2 - \dot{z}_{2d} \\ \dot{z}_3 - \dot{z}_{3d} \end{bmatrix}$ are the position error and velocity error. K_p and K_d are 2 by 2 positive definite diagonal matrix. K_p plays a role as a spring that tries to keep the position error decreasing. K_d is considered as a damper which maintains the velocity error \dot{e} decreasing.

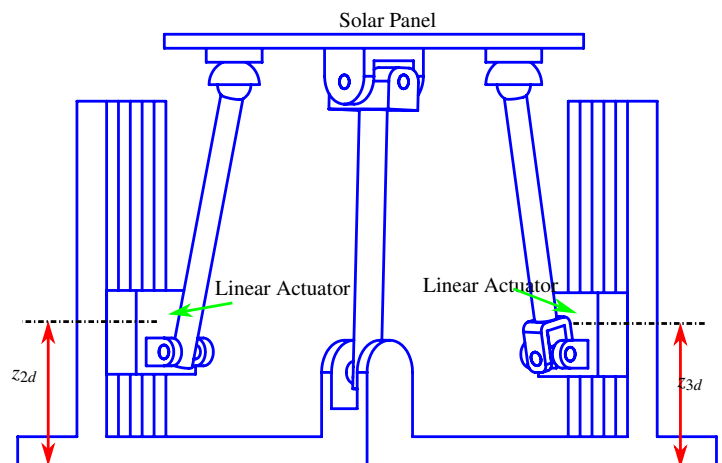


Figure 4: Desired configuration of the solar panel

5 Results and Discussion

PD control law is applied to drive the parallel mechanism from its initial configuration to the desired configuration with $K_p = \begin{bmatrix} 50 & 0 \\ 0 & 50 \end{bmatrix}$, and $K_d = \begin{bmatrix} 20 & 0 \\ 0 & 25 \end{bmatrix}$ as shown in Figure 1 and Figure 4. The control input $u = [f_{2z} \ f_{3z}]^T$ is exerted to the two actuators by assigning the external forces in the vector $g = [f_1^T \ n_1'^T \ \dots \ f_7^T \ n_7'^T]^T$ containing

$$\begin{aligned} f_2 &= [0 \ 0 \ f_{2z}]^T \\ f_3 &= [0 \ 0 \ f_{3z}]^T, \end{aligned} \quad (24)$$

while keeping the remaining components in g to be zero. Other parameters used in this paper are shown in Appendix C. As can be seen in the Figure 5, the two actuators reach the desired position quickly. The movement of the solar panel can be observed in Figure 7. It appears that the parallel mechanism can be easily controlled such that it is practically possible to move the solar panel directed to the sunlight, and thus more energy could be produced. It is evident that the desired orientation of the solar panel is with its coordinate system $(\xi_7\eta_7\zeta_7)$ is parallel to the global coordinate system (xyz) . In this case, the euler parameters is expected to be equal to $[\cos \frac{\phi}{2} \ 0 \ 0 \ \sin \frac{\phi}{2}]^T$ [8], where ϕ is the rotation angle around ζ axis, and is reported true by Figure 8. Figure 9 illustrates the mathematical relationship of euler parameters of the solar panel as described in (1) which satisfies $p_7^T p_7 = 1$. When the euler parameters are used to describe a rotational coordinate, it is important to ensure that (1) is satisfied because the four quantities of euler parameters are not independent.

6 Conclusion

Our study provides the frame work for modeling any mechanism by obtaining the algebraic differential equations of motion derived from Newton-Euler equation of motion and kinematic constraint equations. This technique can be applied to a wide range of simulation applications, especially for a close loop mechanism. Moreover, our result confirms the usefulness of the Baumgarte stabilization method that deals with numerical error when solving system of algebraic differential equations with mathematical constraint of Euler parameters. The control simulations using PD controller was to drive the solar panel to reach the desired configuration with a good performance.

Future work should focus on applying a model based controller that could provide a better control result, especially for tracking control. If the same modeling approach is applied to a system that requires fast response, an investigation on computation time should be made.

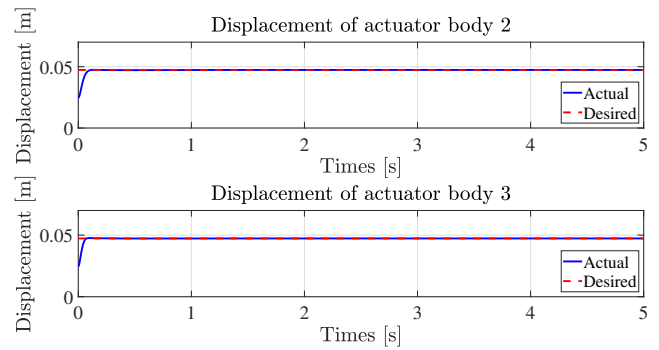


Figure 5: Response of Actuator's Displacement

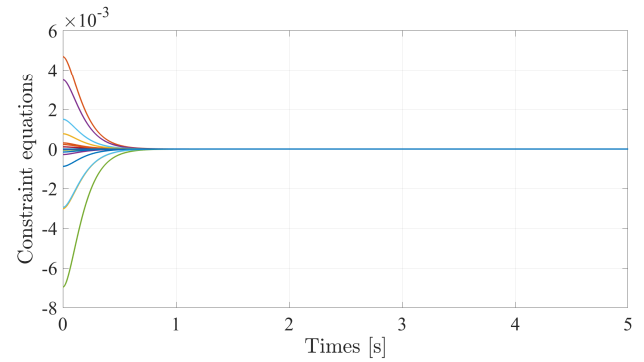


Figure 6: Kinematic constraint

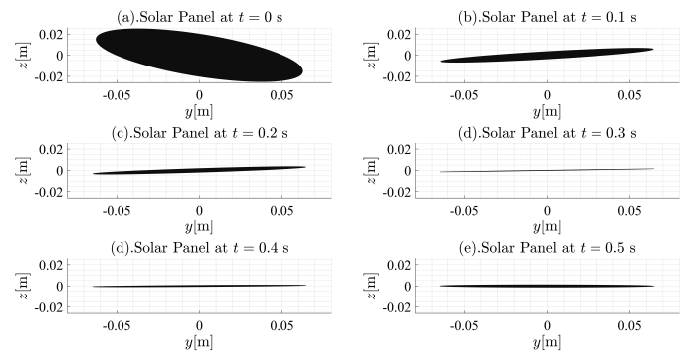


Figure 7: Orientation of Solar Panel

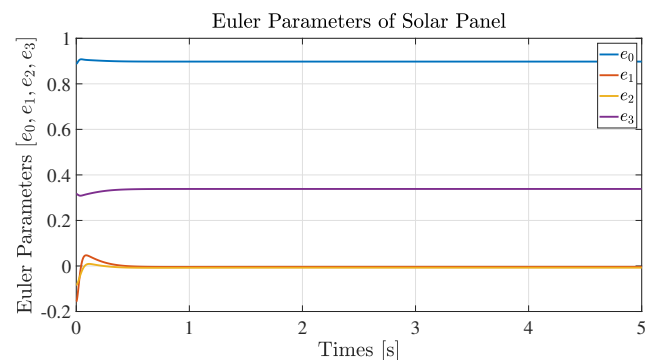


Figure 8: Euler Parameters Describing the Orientation of Solar Panel

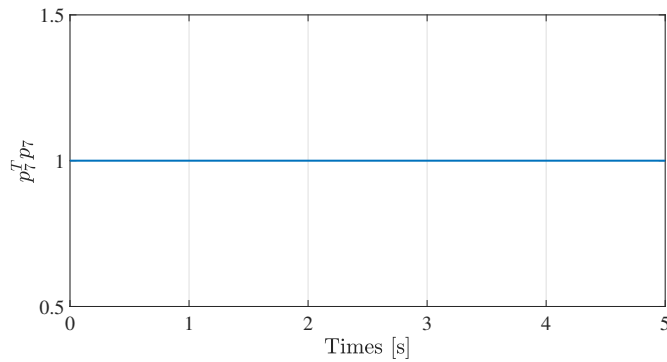


Figure 9: Mathematical Relationship of Euler Parameters of Solar Panel

APPENDIX A

For the parallel mechanism, by following the concept of relative constraints between two bodies from [8], the 34 constraint equations are obtained as follows:

- Four equations for each Universal joint between body (3,5) and (4,7).

$$\begin{aligned}\Phi^{(s,3)} &\equiv r_i + A_i s_i'^P - r_j - A_j s_j'^P = 0 \\ \Phi^{(n1,1)} &\equiv s_i^T s_j = 0,\end{aligned}\quad (26)$$

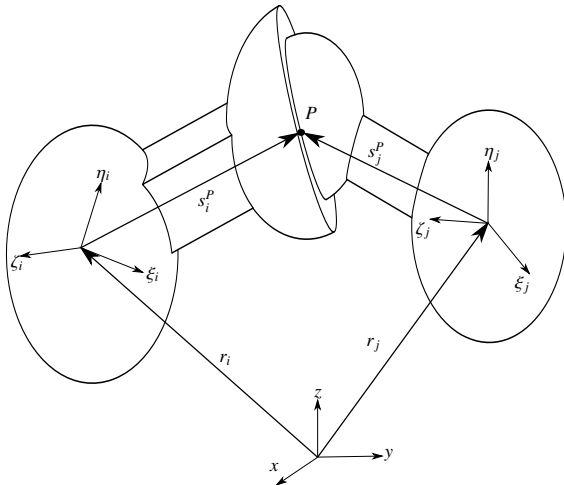


Figure 10: Spherical Joint

- Three equations for each Spherical joint between body (5,7) and (6,7).

$$\Phi^{(s,3)} \equiv r_i + A_i s_i'^P - r_j - A_j s_j'^P = 0, \quad (25)$$

where $s_i'^P = [\xi^P, \eta^P, \zeta^P]$ is body-fixed coordinate of the point P .

$$\begin{aligned}\Phi^{(s,3)} &\equiv r_i + A_i s_i'^P - r_j - A_j s_j'^P = 0 \\ \Phi^{(n1,1)} &\equiv s_i^T s_j = 0,\end{aligned}\quad (26)$$

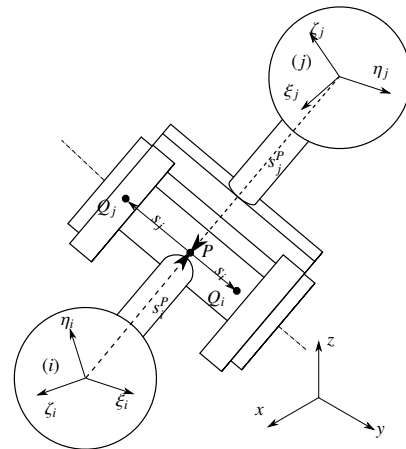


Figure 12: Revolute Joint

- Five equations for each Revolute joint between body (1,4) and (2,6).

$$\begin{aligned}\Phi^{(s,3)} &\equiv r_i + A_i s_i'^P - r_j - A_j s_j'^P = 0 \\ \Phi^{(p1,2)} &\equiv \tilde{s}_i s_j = 0,\end{aligned}\quad (27)$$

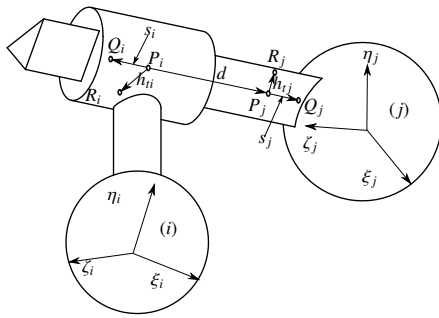


Figure 13: Translational Joint

• Five equations for each Translational joint between body (1,2) and (1,3).

$$\begin{aligned}\Phi^{(p1,2)} &\equiv \tilde{s}_i s_j = 0 \\ \Phi^{(p2,2)} &\equiv \tilde{s}_i d = 0 \\ \Phi^{(n1,1)} &\equiv h_{ti}^T h_{tj} = 0,\end{aligned}\quad (28)$$

APPENDIX B

Consider the following mass spring damper equation of motion

$$\ddot{D} + 2\zeta\omega_n\dot{D} + \omega_n^2 D = 0, \quad (29)$$

where ζ is a critical damping constant, and ω_n denotes a natural frequency. From (6) and (29), we can write

$$\begin{aligned}\ddot{D} + K_D\dot{D} + K_P D &= 0 \\ \ddot{D} + 2\zeta\omega_n\dot{D} + \omega_n^2 D &= 0\end{aligned}\quad (30)$$

$$\begin{aligned}\zeta &= \frac{K_D}{2\omega_n} = \frac{K_D}{2\sqrt{K_P}} \\ \omega_n &= \sqrt{K_P}\end{aligned}\quad (31)$$

In the case of critically damped system, $\zeta = 1$ ensures a fast response with no overshoot. Therefore, we choose $K_D = 2\alpha$ and $K_P = \alpha^2$, where α is a positive constant and taken to be 10.

APPENDIX C

Table 1: Mass of body $i, i = 1, 2, \dots, 7$.

Symbols	Value	Unit
m_1	475.09×10^{-3}	Kg
m_2	189.7×10^{-3}	Kg
m_3	189.7×10^{-3}	Kg
m_4	104.45×10^{-3}	Kg
m_5	53.25×10^{-3}	Kg
m_6	54.4×10^{-3}	Kg
m_7	890.5×10^{-3}	Kg

Table 2: Position vector of center of mass of body i at initial position, $i = 1, 2, \dots, 7$

Symbols	Value	Unit
r_1	$10^{-3} \times [-63.93, 63.93, 30.41]^T$	m
r_2	$10^{-3} \times [-123.99, 15, 24.6]^T$	m
r_3	$10^{-3} \times [-15, 123.99, 24.6]^T$	m
r_4	$10^{-3} \times [-11.50, 18.37, 99.21]^T$	m
r_5	$10^{-3} \times [-12.99, 98.33, 68.84]^T$	m
r_6	$10^{-3} \times [-92.31, 15, 66.27]^T$	m
r_7	$10^{-3} \times [-34.28, 42.89, 136.56]^T$	m

Table 3: Euler parameters of body i at initial position, $i = 1, 2, \dots, 7$

Symbols	Value
p_1	$[1, 0, 0, 0]^T$
p_2	$[1, 0, 0, 0]^T$
p_3	$[1, 0, 0, 0]^T$
p_4	$[1, 0, 0, 0]^T$
p_5	$[1, 0, 0, 0]^T$
p_6	$[1, 0, 0, 0]^T$
p_7	$[0.89043, -0.19791, -0.10481, 0.39619]^T$

Table 4: Moment of Inertia of body $i, i = 1, 2, \dots, 7$

Symbols	Value	Unit
J'_1	$10^{-4} \times \begin{bmatrix} 20 & 8 & -1 \\ 8 & 20 & 1 \\ 1 & 1 & 26 \end{bmatrix}$	Kg m ²
J'_2	$10^{-4} \times \begin{bmatrix} 0.2774 & 0 & -0.0102 \\ 0 & 0.2015 & 0 \\ -0.0102 & 0 & 0.1987 \end{bmatrix}$	Kg m ²
J'_3	$10^{-4} \times \begin{bmatrix} 0.2015 & 0 & 0 \\ 0 & 0.2774 & 0.0102 \\ 0 & 0.0102 & 0.1987 \end{bmatrix}$	Kg m ²
J'_4	$10^{-3} \times \begin{bmatrix} 0.1217 & 0.0000 & 0 \\ 0.0000 & 0.1248 & 0 \\ 0 & 0 & 0.0054 \end{bmatrix}$	Kg m ²
J'_5	$10^{-4} \times \begin{bmatrix} 0.5827 & 0 & -0.0824 \\ 0 & 0.5940 & 0 \\ -0.0824 & 0 & 0.0172 \end{bmatrix}$	Kg m ²
J'_6	$10^{-4} \times \begin{bmatrix} 0.6242 & 0 & 0 \\ 0 & 0.6231 & -0.0000 \\ 0 & -0.0000 & 0.0058 \end{bmatrix}$	Kg m ²
J'_7	$10^{-4} \times \begin{bmatrix} 12 & 0 & 1 \\ 0 & 12 & 0 \\ 1 & 0 & 24 \end{bmatrix}$	Kg m ²

Acknowledgment This material is based upon work supported by the Air Force Office of Scientific Research under award number FA2386-17-1-0148.

References

- [1] S. Srang and S. Ath, "Dynamic Modeling and Simulation for 2DOF Parallel Mechanism Solar Tracker," 2019 IEEE/ASME International Conference on

- Advanced Intelligent Mechatronics (AIM), Hong Kong, China, 283-288, 2019. <https://doi.org/10.1109/AIM.2019.8868501>
- [2] C.S. Chin, A. Babu, W. McBride, "Design, modeling and testing of a standalone single axis active solar tracker using MATLAB/Simulink", *Renewable Energy*, **36**(11), 3075-3090, 2011. <https://doi.org/10.1016/j.renene.2011.03.026>
- [3] Yingxue Yao, Yeguang Hu, Shengdong Gao, Gang Yang, Jinguang Du, "A multipurpose dual-axis solar tracker with two tracking strategies", *Renewable Energy*, **72**, 88-98, 2014. <https://doi.org/10.1016/j.renene.2014.07.002>
- [4] P. Y. Vorobiev, J. Gonzalez-Hernandez and Y. V. Vorobiev, "Optimization of the solar energy collection in tracking and non-tracking photovoltaic solar system," (ICEEE). 1st International Conference on Electrical and Electronics Engineering, 2004., Acapulco, Mexico, 310-314, 2004. <https://doi.org/10.1109/ICEEE.2004.1433900>
- [5] Hossein Mousazadeh, Alireza Keyhani, Arzhang Javadi, Hossein Mobli, Karen Abrinia, Ahmad Sharifi, "A review of principle and sun-tracking methods for maximizing solar systems output", *Renewable and Sustainable Energy Reviews*, **13**(8), 1800-1818, 2009. <https://doi.org/10.1016/j.rser.2009.01.022>
- [6] T. Zhan, W. Lin, M. Tsai and G. Wang, "Design and Implementation of the Dual-Axis Solar Tracking System," 2013 IEEE 37th Annual Computer Software and Applications Conference, Kyoto, 276-277, 2013. <https://doi.org/10.1109/COMPSAC.2013.46>
- [7] J. Wu, X. Chen and L. Wang, "Design and Dynamics of a Novel Solar Tracker With Parallel Mechanism," in *IEEE/ASME Transactions on Mechatronics*, **21**(1), 88-97, Feb. 2016. <https://doi.org/10.1109/TMECH.2015.2446994>
- [8] Nikravesh, Parviz E. Computer-aided analysis of mechanical systems, Prentice-Hall, Inc., 1988.
- [9] Neto, M.A., Ambrósio, J. "Stabilization Methods for the Integration of DAE in the Presence of Redundant Constraints". *Multibody System Dynamics* **10**, 81-105 (2003). <https://doi.org/10.1023/A:1024567523268>
- [10] Flores, P., Machado, M., Seabra, E., and Tavares da Silva, M. (October 13, 2010). "A Parametric Study on the Baumgarte Stabilization Method for Forward Dynamics of Constrained Multibody Systems." *ASME. J. Comput. Nonlinear Dynam.* January 2011; **6**(1): 011019. <https://doi.org/10.1115/1.4002338>
- [11] Flores P., Pereira R., Machado M., Seabra E. (2009) "Investigation on the Baumgarte Stabilization Method for Dynamic Analysis of Constrained Multibody Systems". In: Ceccarelli M. (eds) *Proceedings of EUCOMES 08*. Springer, Dordrecht. <https://doi.org/10.1007/978-1-4020-8915-2-37>